Simulation of Hot-Electron Effects with Multi-band Semiconductor Devices

Lars P. Tatum, Madeline Sciullo, Mark E. Law
Department of Electrical and Computer Engineering
University of Florida
Gainesville, FL, USA
ltatum@ufl.edu

Abstract— **In this work, we present a 2-Valley energy band model of electron transport that delivers more accurate solutions compared with the Farahmand model but with improved convergence and a faster solution time for very high electric fields. This was achieved by implementing the Fermi-Dirac integral distribution as a substitution for the Boltzmann exponential, electron carrier temperature due to heat generation and conduction in the semiconductor lattice, and additional electron concentration modeling for a second conduction energy band minima. The model was primarily tuned by varying the electron temperature relaxation time constant. It was tested using a GaN-based High Electron Mobility Transistor using the Finite-Element Quasi Fermi method.**

Keywords— electron mobility, electron temperature, Fermi-Dirac, 2-Valley, HEMT, Gallium Nitride, high electric field, multiband model, hot carrier effects

I. Introduction

In some scaled semiconductor devices and materials, the electric field can become strong enough to scatter electrons into higher energy conduction bands. Materials with wide energy band gap structures such as Gallium Nitride are highly susceptible to this effect since their applications involve high electric fields. If the higher energy band has a larger electron effective mass, this can significantly degrade device response. Today's numerical models make use of an empirical relationship between electron velocity and electric field to try and account for this scattering. Modeling this is a challenge as there are no a-priori relationships between velocity and field and this is needed to further develop numerical solutions.

This issue has been addressed in literature with a few different approaches. Some have simplified the picture and assumed a constant mobility and saturation velocity rather than dealing with a complex expression for mobility that accounts for scattering effects[1][2]. In situations where it was imperative to have a highly accurate mobility, complex expressions were used with limited results due to convergence issues[3]. Others have tackled these effects using complex mobility models based on temperature or electric field[4][5], while some have settled for using the low-field mobility to approximate the behavior[6].

Few have attempted to account for these effects using a multiband model. S. Vitanov et al. [7] used a two valley hydrodynamic mobility model to describe high field behavior by defining 2 valley-specific mobilities and taking a weighted mean, with the weighting determined by valley specific parameters. They obtained acceptable results in comparison to Monte-Carlo methods. However, their work is more focused on the modeling of hot-carrier effects on mobility.

To understand these issues, we have explored and implemented additional phenomena, including the Fermi-Dirac integral distribution, carrier temperature due to heat generation and conduction in the semiconductor lattice, and multiple band energy levels, all of which result in a more physical approach. These additions were applied and demonstrate an increased accuracy in computing quasi-Fermi levels, increased likelihood for convergence, and quicker solution time as compared to conventional modeling techniques using complex mobility-field relationships.

II. Simulation Methodology

A. Overview

Steady-state device simulations were carried out using the FLorida Object Oriented Device Simulator (FLOODS). The Finite element quasi-Fermi (FEQF) approach was used to solve partial differential equations for electron and hole quasi-Fermi level continuity and electrostatic potential[8]. The FEQF approach was chosen in this situation to allow for the simple extrapolation of electron concentration in both valleys given one partial differential equation for the electron quasi-Fermi level.

B. Fermi-Dirac Integral

The Fermi-Dirac (F-D) distribution was added as opposed to the more commonplace Boltzmann distribution to calculate the electron concentration from the quasi-Fermi level. The F-D distribution better captures carrier concentrations when the quasi-Fermi level is near or above the conduction band edge as is found in most High Electron Mobility Transistor (HEMT) devices. The F-D Integral was defined and calculated in a computationally efficient manner using the short series approximations laid out by P. Van Halen and D. L. Pulfrey, which have an error of less than 10^{-5}[9], [10].

C. Heat Generation and Conduction

Next, heat generation and conduction relationships were implemented to calculate electron temperature fluctuations independent of the lattice temperature. The carriers and the lattice are treated as their own thermodynamic subsystems[11]. Modeling carrier thermodynamics in this way allows the thermal energy of electrons to be more accurately calculated, which becomes especially relevant in high electric field conditions. Hot carrier effects resulting from high electron temperatures are the basis for scattering into upper conduction bands and contribute to the interesting nonlinear mobility effects in multiband devices. Electron temperature is used to couple the two valleys in this approach, as it largely dictates the electron population distributions. Individual parameters such as the electron relaxation time were tuned accordingly to best match results using the Farahmand mobility model as reference.

D. 2-Valley Energy Bands

Under a high electric field, electrons will heat up as they gain more energy and scatter off the lattice. As electrons' temperature increases, they will begin to scatter to higher energy conduction bands. A strong electric field excites the electrons and can provide enough energy to scatter them into the upper conduction bands. In these upper conduction bands, electron transport properties can change drastically. For GaN in particular, electron effective mass increases significantly in the upper bands [12], which results in a reduced drift velocity for those electrons. In turn, the average drift velocity of the electrons (accounting for all conduction bands) can decrease as more electrons are excited into upper bands. To calculate electron concentrations in the upper bands, the aforementioned Fermi-Dirac integral distribution, denoted in the equations below as $F_{1/2}$, with the calculated electron temperature is used to determine the electron concentrations. The electron energy relaxation with the lattice allows the carrier to scatter back into lower energy levels.

$$n_1 = N_{c1} * F_{1/2}\left(\frac{\phi_n - E_c}{kT_{elec}}\right)$$

$$n_2 = N_{c2} * F_{1/2}\left(\frac{\phi_n - E_c - \Delta E_g}{kT_{elec}}\right)$$

The second band is differentiated from the first band using a higher energy level (ΔE_g) in addition to the new density of states in the second band that can be estimated from the change in effective mass[13]. This two-valley model was implemented only for the GaN material. The second valley is incorporated in the partial differential equation for the GaN's electron quasi-Fermi level as follows, where n is simply the sum of the two electron concentrations computed from each energy band:

$$\frac{\partial n}{\partial t} = \mu_1 n_1 \nabla\phi_n + \mu_2 n_2 \nabla\phi_n$$

as opposed to the typical expression:

$$\frac{\partial n}{\partial t} = \mu n \nabla\phi_n$$

The same Caughey-Thomas lattice temperature-dependent low field mobility equation was used for the electron mobility in both bands. Upper-band mobility is scaled using the electron effective mass; transport differences are captured from differences in electron effective mass and electron concentrations.

Since electron drift is the dominant form of carrier transport in the HEMT structure used, the 2 valley model was only applied to the conduction energy bands, and the hole mobility was left constant.

E. Benchmarking

This modeling approach was compared with the well-accepted Farahmand Model for electron mobility in GaN. The Farahmand model of transport dynamics for III-nitride compounds is based on Monte Carlo simulations for major scattering mechanisms[4]. The Farahmand model's parameters are tuned to match experimental data to develop a field dependent mobility relationship for GaN and other materials. The Farahmand empirical mobility model can be used to develop a field-dependent drift velocity model as depicted in Figure 1.

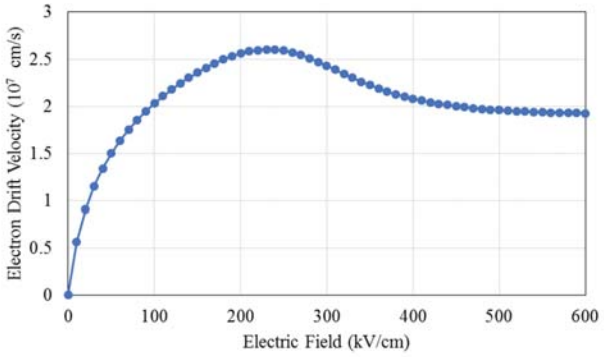

Figure 1: Farahmand Empirical model for Electron Drift Velocity

The velocity-field relationship in Figure 1 can lead to convergence issues in simulations due to the decrease in velocity with increase in electric field past the peak drift velocity. The models we used are compared in the following table:

TABLE I. KEY EQUATIONS IMPLEMENTED

Farahmand Model	2-Valley Model
• Poisson Equation • Electron Continuity Equation • Hole Continuity Equation • Farahmand field dependent mobility model • Boltzmann distribution	• Poisson Equation • Electron Continuity Equation • Hole Continuity Equation • Band-dependent mobility model • Fermi-Dirac integral statistics for 2 valleys • Electron Temperature thermodynamics

Figure 2 diagrams the test AlGaN/GaN HEMT model of gate length 1 micron that was used to compare the performance of the two simulation models. The HEMT is a suitable device to test these high-field models because it's designed to handle high power due to its wide bandgap, regularly reaching high-field saturation conditions during operation.

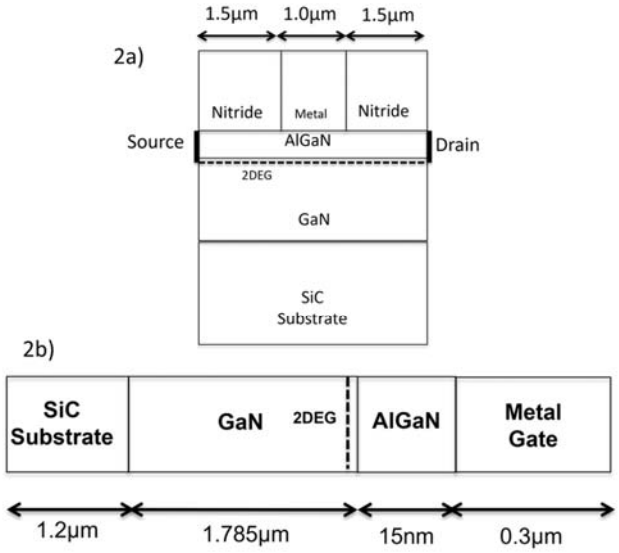

Figure 2a: 2D view of the HEMT test structure

Figure 2b: Vertical cross section of HEMT test structure.

III. Results

In this study, the HEMT drain voltage was swept while keeping the gate voltage constant at 0V, and the corresponding drain current was computed using both modeling approaches.

The electron scattering relaxation time pertinent to the 2-Valley model, τ, was tuned to find a match between the current-voltage (I-V) characteristics of the two models. As seen in Figure 3, larger values of τ cause the current to rolloff (start decreasing) at a smaller bias voltage while smaller values cause the opposite to occur. Another general trend observed is for shorter relaxation times, the curve seems to smoothen out, achieving better convergence. A value of 2 picoseconds best matches the Farahmand model; the two I-V curves are compared in Figure 4. Figure 4 also shows the convergence issue of the Farahmand model, where the simulation cannot converge past roughly 2.75V whereas the 2-Valley model converges well past it at roughly 8V.

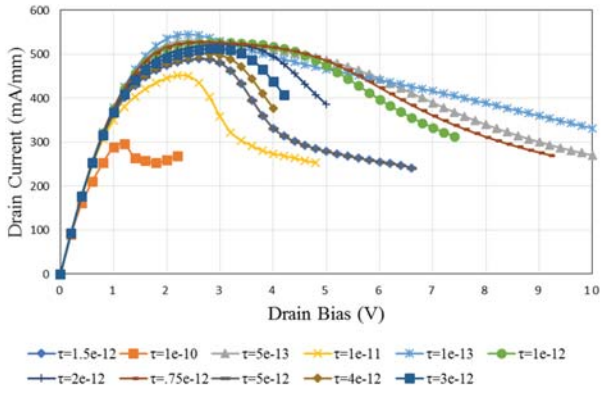

Figure 3: 2-Valley IV curves with varying τ

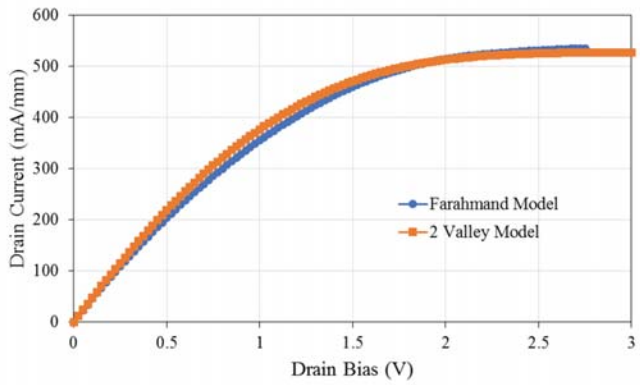

Figure 4: Matched I-V curves for the Farahmand and 2 Valley models

As the drain bias increased, the second band's electron concentration increased, especially in the channel under the gate. Notably, some peaking occurred under the gate, especially at the drain end of the gate where the concentration in both bands skyrockets. In this bottlenecked region, the concentration in the second band becomes greater than the first, which correlates strongly with the decreasing current seen at high bias. The two conduction band populations evolve as shown in Figure 5.

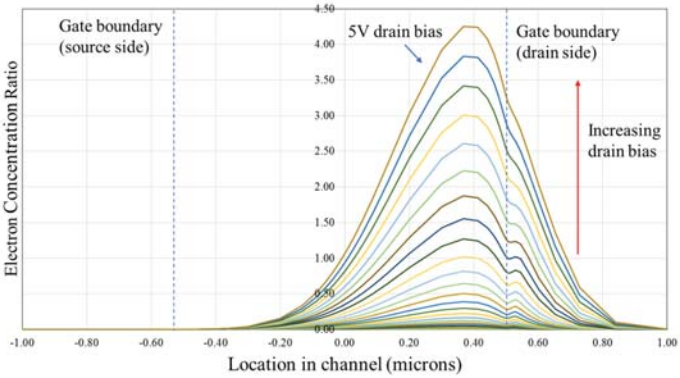

Figure 5: Electron Concentration in band 2 w.r.t. band 1 as bias is increased

Since the two-valley model involves solving for an extra partial differential equation for electron temperature, the hypothesis was that the two-valley model would show longer computation time and some possible convergence issues commonly related to having to solve for an additional partial differential equation. However, the 2-Valley model showed steady convergence, up to around 8V, with the chosen relaxation constant, while the Farahmand model stopped converging at a drain bias of 2.75V, shown in Figure 4. The solution time at each bias point was also recorded and tallied up. The 2-Valley model has an approximately bias independent solution time whereas the Farahmand model's solution time increases as the drain bias is stepped up until it levels off at about 1.8V (Figure 6). Moreover, the Farahmand model has an exponentially increasing cumulative solution time, whereas the 2-Valley model results in a more linear increase in solution time (Figure 7).

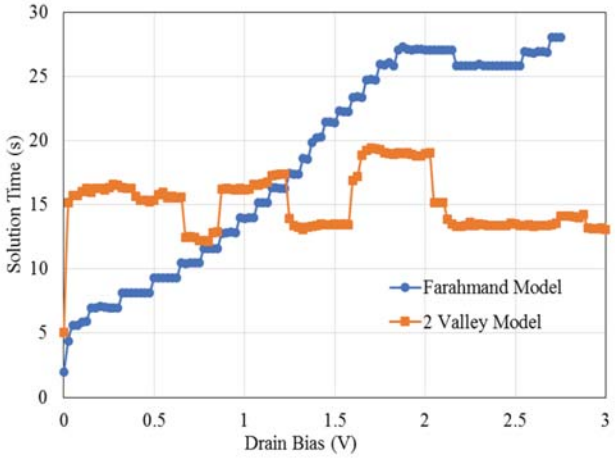

Figure 6: Solution time at each bias step

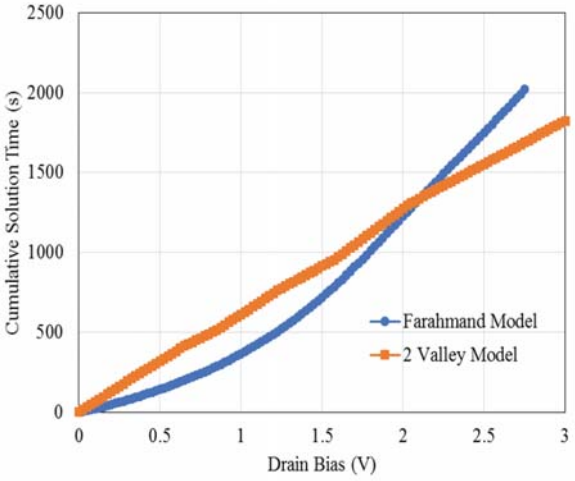

Figure 7: Cumulative solution time

IV. Conclusions

In conclusion, the 2-Valley model developed delivers similar results as the Farahmand model but with better convergence and a faster solution time. This was achieved by modeling the Fermi-Dirac integral distribution, carrier temperature due to heat generation and conduction in the semiconductor lattice, and multiple energy bands. The model was primarily tuned by varying the electron relaxation time. It was tested on a GaN-based High Electron Mobility Transistor using the Finite-Element Quasi Fermi method.

Future work will include tuning of other thermal transport related parameters to better capture more of the heat generation physics and have a more precise model of electron temperature. It will also be insightful to benchmark the 2-Valley model against the Farahmand model implemented using the Scharfetter-Gummel discretization, work that is currently in progress. The 2-Valley model could also be extended to modeling other materials beyond GaN or other devices beyond the HEMT which was tested in this study.

References

[1] J. M. Tirado, J. L. Sánchez-Rojas, and J. I. Izpura, "Trapping effects in the transient response of AlGaN/GaN HEMT devices," *IEEE Trans. Electron Devices*, vol. 54, no. 3, pp. 410–417, 2007.

[2] H. Zhao, G. Liu, R. A. Arif, and N. Tansu, "Current injection efficiency induced efficiency-droop in InGaN quantum well light-emitting diodes," *Solid. State. Electron.*, vol. 54, no. 10, pp. 1119–1124, 2010.

[3] E. E. Patrick, M. Choudhury, F. Ren, S. J. Pearton, and M. E. Law, "Simulation of Radiation Effects in AlGaN/GaN HEMTs," *ECS J. Solid State Sci. Technol.*, vol. 4, no. 3, pp. Q21–Q25, 2015.

[4] M. Farahmand *et al.*, "Monte Carlo simulation of electron transport in the III-nitride Wurtzite phase materials system: Binaries and ternaries," *IEEE Trans. Electron Devices*, vol. 48, no. 3, pp. 535–542, 2001.

[5] A. Kumar and M. M. De Souza, "Modelling the threshold voltage of p-channel enhancement-mode GaN heterostructure field-effect transistors," *IET Power Electron.*, vol. 11, no. 4, 2018.

[6] W. Ying, X. Likun, and D. Kun, "Improved trench MOS barrier Schottky rectifier by dielectric engineering," *IET Power Electron*, vol. 7, no. 2, pp. 325–329, 2014.

[7] S. Vitanov, V. Palankovski, S. Maroldt, and R. Quay, "High-temperature modeling of AlGaN/GaN HEMTs," *Solid. State. Electron.*, vol. 54, no. 10, pp. 1105–1112, 2010.

[8] D. J. Cummings, M. E. Law, S. Cea, and T. Linton, "Comparison of discretization methods for device simulation," *Int. Conf. Simul. Semicond. Process. Devices, SISPAD*, 2009.

[9] P. Van Halen and D. L. Pulfrey, "Accurate, short series approximations to Fermi-Dirac integrals of order -1/2, 1/2, 1, 3/2, 2, 5/2, 3, and 7/2," *J. Appl. Phys.*, vol. 57, no. 12, pp. 5271–5274, 1985.

[10] P. Van Halen and D. L. Pulfrey, "Erratum: "Accurate, short series approximation to Fermi-Dirac integrals of order -1/2, 1/2, 1, 3/2, 2, 5/2, 3, and 7/2" (Journal of Applied Physics (1985) 57, (5271))," *J. Appl. Phys.*, vol. 59, no. 6, pp. 2264–2265, 1986.

[11] G. K. Wachutka, "Rigorous thermodynamic treatment of heat generation and conductionin semiconductor device modeling," *Comput. Des. Integr. Circuits Syst. IEEE Trans.*, vol. 9, no. I, pp. 1141–1149, 1990.

[12] M. Goano, E. Bellotti, E. Ghillino, C. Garetto, G. Ghione, and K. F. Brennan, "Band structure nonlocal pseudopotential calculation of the III-nitride wurtzite phase materials system. Part II. Ternary alloys AlxGa1-xN, InxGa1-xN, and InxAl1-xN," *J. Appl. Phys.*, vol. 88, no. 11, pp. 6476–6482, 2000.

[13] M. Goano, E. Bellotti, E. Ghillino, C. Garetto, G. Ghione, and K. F. Brennan, "Band structure nonlocal pseudopotential calculation of the III-nitride wurtzite phase materials system. Part I. Binary compounds GaN, AlN, and InN," *J. Appl. Phys.*, vol. 88, no. 11, pp. 6476–6482, 2000.